40th Joint Propulsion Conference
Fort Lauderdale, Florida
July 11-14, 2004

AIAA-2004-3432

Measurement of Ion Energy Distributions Produced within an NSTAR Discharge Chamber

Casey C. Farnell* and John D. Williams†
Colorado State University, Fort Collins, 80523

Measurements are presented of ion energy distributions produced within a prototype NSTAR discharge chamber as a function of its operational parameters. The goal of this effort is to document the ion energy distribution characteristics and determine features that could cause rapid sputter erosion of discharge chamber components. Ion energy distributions were measured with a Comstock model AC-901 electrostatic analyzer (ESA) that was located outside of the discharge chamber and sighted through a slit that was cut in the side of the anode and along a diameter across the pseudo-screen grid. Important results are that, at some locations within the discharge chamber at high discharge current operating conditions, high energy ion groups (with drift energies of order 100 eV that are separate and distinct from groups at the discharge energy) can be produced that would cause rapid sputter erosion to most discharge chamber thruster components comprised of molybdenum, stainless steel, tantalum, and tungsten. Under nominal operating conditions, no significant high-energy groups (separate from the discharge ion signal) are detected. However, high energy tails on the discharge ion signal are detected that display effective temperatures of order 10 eV. An additional result is that the discharge ion signal appears to be Maxwellian and ion temperatures of 3 to 4 eV have been measured. In some situations, the discharge ion signal is much stronger than high energy ion groups present to the extent that the discharge ion group tail would cause more sputter erosion than the high energy group (at the location of the ESA).

I. Introduction

Ion engines utilize hollow cathodes as the electron source used to drive discharge plasma production. During extended life tests performed on NASA's NSTAR flight spare ion engine, components at and near the hollow cathode have been observed to be completely eroded away[1] presumably due to sputter erosion by energetic or multi-charged ion bombardment. Although highly eroded during the test, this thruster processed over three times the on-mission propellant of its flight twin. The very successes of NASA's NSTAR flight and life test thrusters have opened the door to the consideration of much more demanding missions for ion thrusters and their hollow cathode components. As spacecraft become larger and missions become more ambitious, it is necessary to increase the lifetimes of hollow cathodes and the components near them while simultaneously exposing them to progressively harsher operational conditions.[2,3,4] The focus of this work is to characterize the energy distribution of ions produced within the discharge chamber especially in regions nearby the hollow cathode. The long term goal of this work is to understand the mechanisms of how ions (possibly multi-charged) gain sufficient energy to sputter erode components. The hope is that once these mechanisms are understood through careful experimental measurements, they can be mitigated. If this is not possible, a deeper understanding of the discharge plasma flow field properties may enable one to specify the requirements of a sputter resistant component that could be placed near the cathode as a sacrificial remedy for a given discharge chamber operating condition.

In previous work conducted in our laboratory,[5] we have investigated the characteristics of high energy ions using a remotely located electrostatic analyzer (ESA). High energy ions were observed to flow from regions near the hollow cathode assembly. These observations include measurement of ions that have "through anode" energies and beyond, that show ion energies increasing as flow rate is reduced, and that have more energetic ion production as the discharge current is increased. Interestingly, more energetic ions were detected when the ESA was sighted

* Graduate Research Assistant, Mechanical Engineering, 1320 Campus Delivery, AIAA Student Member
† Assistant Professor, Mechanical Engineering, 1320 Campus Delivery, AIAA Senior Member

along zenith angles between 20 and 90 degrees and along a line-of-sight slightly behind or beside the cathode orifice for any given operating condition.

In this paper, we will present improved data collected with the ESA over a range of cathode flow rate and discharge current. After a period of a few hours of continuous use, the ESA probe would begin to malfunction. The symptoms included significant reductions in the ion current signal and a poor ability to reproduce ion energy distribution functions at a given operating condition. The improvements in data quality were obtained by carefully cleaning the probe between tests and periodically checking its operation against a well-understood mono-energetic ion source.

II. Experimental Apparatus and Test Procedures

A schematic of the experimental setup is shown in Fig. 1 along with a photograph of the experiment as it was installed in one of the vacuum systems at CSU. As shown in the schematic, a hollow cathode was used to supply electrons to the discharge chamber that was fabricated to be similar to the 30-cm diameter NSTAR discharge chamber. Three magnet rings were used to produce the magnetic field. The first was located near the exit of the source (where the ion optics would be located on an actual NSTAR ion engine) at one end of the cylindrical side-wall section, the second was placed at the intersection of the cylindrical and conical anode sections, and the third behind the cathode on the back plate. The discharge chamber body was fabricated out of aluminum where the inside surface was covered with a stainless steel lining. Although no ion optics system was present, a pseudo-screen grid was placed where the ion optics would normally be located. This was done to enable operation of the discharge chamber at plasma and neutral densities similar to the NSTAR engine.

To measure the energy characteristics of ions produced within the discharge chamber, a slot, 7 mm in width, was cut along the side of the anode and pseudo-screen grid so the plasma produced within the discharge chamber could flow out into the surrounding vacuum regions. An electrostatic analyzer (ESA) was used to measure ion energy distributions. An actuator system was used to position the ESA radially (across a diameter of the chamber) and set the zenith angle of the probe collimator (relative to the discharge chamber axis). The combination of being able to rotate the discharge chamber and move and rotate the ESA allowed for investigation of the energy distributions of ions that flow from different regions and directions within the discharge chamber.

The hollow cathode was operated in an enclosed keeper configuration. The cathode had a tube diameter of 6.3 mm and contained a tungsten insert with low work function material. The cathode orifice was 0.55 mm in diameter. The cathode was heated with a resistive coil wrapped around the cathode tube and the heater was insulated with tantalum foil. The keeper and cathode orifice plates were separated by about 0.5 mm and the keeper orifice diameter was about 2.54 mm. Instead of having separate cathode and main flow as in a typical NSTAR discharge chamber, all of the xenon propellant in this experiment was sent through the cathode.

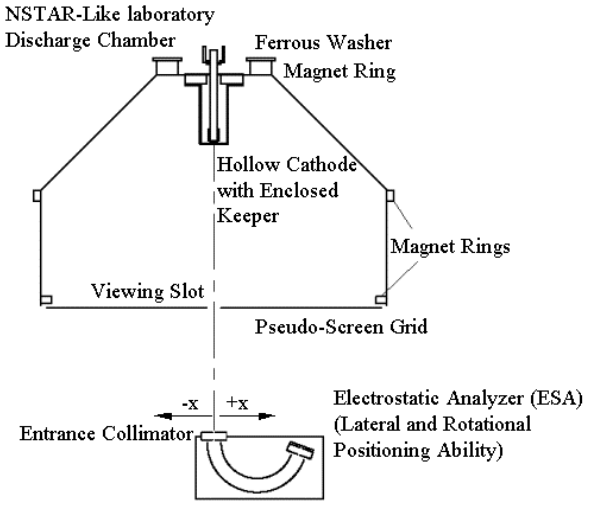

Fig. 1a Schematic of prototype NSTAR discharge chamber.

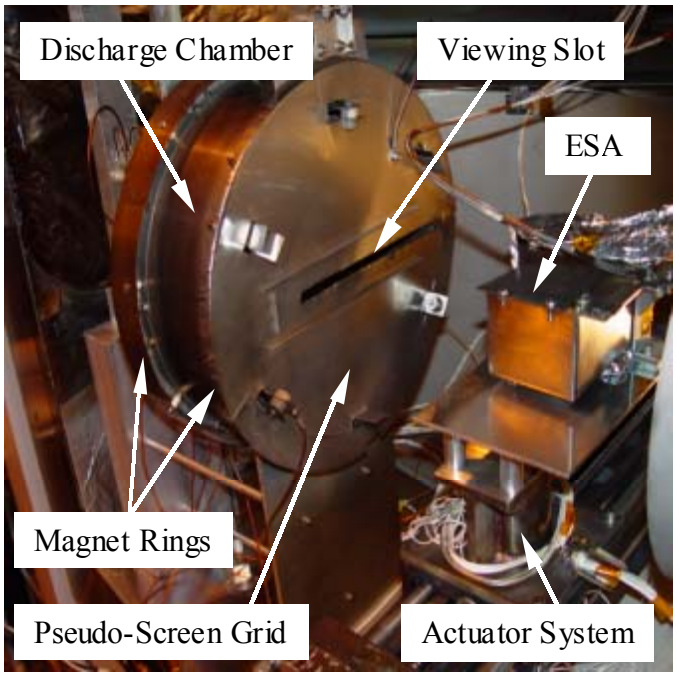

Fig. 1b Photograph of experimental apparatus.

Verification of NSTAR-like Behavior of the Prototype Discharge Chamber

The discharge chamber used in this experiment was similar in shape and function to the NSTAR discharge chamber. The goal of the research presented here was to measure ion energies that would be produced within a realistic thruster configuration, and tests were conducted to determine how well the operating characteristics of the prototype matched the operation of an NSTAR engine. The prototype discharge chamber had about the same dimensions as the NSTAR engine, used similar materials (i.e., non-magnetic side and end walls), had an enclosed keeper around the cathode, and incorporated similar magnetic fields that were produced using three rings of samarium magnets. However, the experimental discharge chamber did not have a set of ion optics (so there was no beam extraction during operation), used only cathode flow (no main flow), and neutral and ion propellant loss was limited to occur through the slots in the side wall and pseudo screen grid instead of through an ion optics assembly.

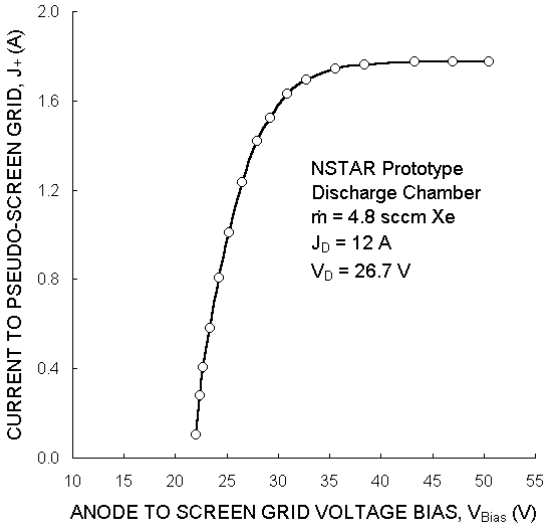

Fig 2a Saturation current to the pseudo-screen grid.

A test was performed to measure the amount of ion current that could be drawn to the pseudo-screen grid at different discharge currents and flow rates. Then, these currents could be compared to the beam current of the NSTAR engine at similar conditions. This test enabled a comparison of efficiently and plasma production rates between a typical NSTAR discharge chamber and the prototype. Figure 2a shows a plot of current to the pseudo-screen grid as a function of bias voltage. As the screen grid was biased more and more negative of the plasma, the ion current increased until it saturated. This saturation current was recorded at different operating conditions and these results are plotted in Figs. 2b, and 2c. Figure 2b shows the ion current to the screen grid as a function of discharge current at three different flow rate values. The three flow rates of 4.8, 6.2, and 7.6 sccm Xe were chosen to maintain the discharge voltage in the range of 20 to 30 V. As the discharge current was increased from 8 to 16 A, the amount of current

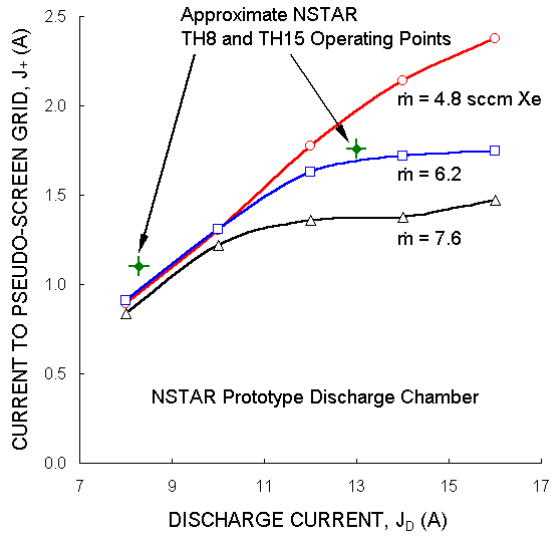

Fig. 2b NSTAR-like discharge chamber beam current comparison.

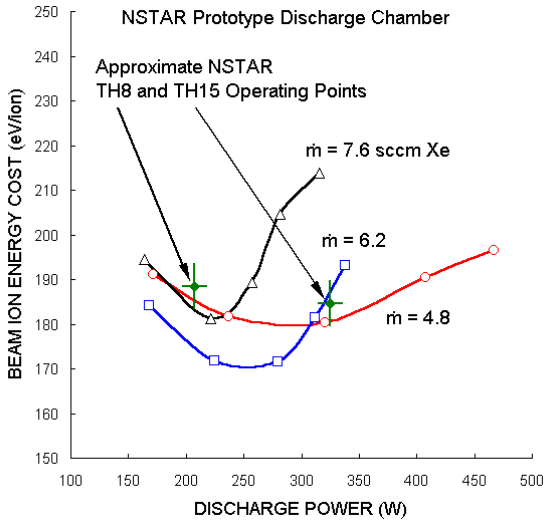

Fig. 2c Beam ion energy cost comparison for the NSTAR-like discharge chamber.

that could be drawn to the screen increased from about 0.84 A to a maximum of 2.38 A at the 4.8 sccm flow. For comparison, the beam currents at the TH8 and TH15 throttle points are plotted at their appropriate discharge current levels and were found to be in reasonable agreement with the prototype measurements. Figure 2c is a plot of the beam ion energy cost (eV/ion) versus discharge power (W). Again, the TH8 and TH15 throttle points are plotted for comparison to the measured values. The beam ion energy cost varied from about 170 to 215 eV/ion for the operating points tested. For most of the discharge power points, the beam ion cost was the lowest for the 6.2 sccm flow rate and highest for the 7.6 sccm flow rate. These beam ion costs seem to be reasonable when compared to those for the TH 8 and TH15 operating points, which had ion energy costs of about 180 to 190 eV/ion. As mentioned above, the goal of these tests was to determine if the prototype discharge chamber was operating similar to an NSTAR engine in terms of plasma production levels. During the testing using the ESA and other probes, an effort was made to maintain reasonable operating conditions (cathode flow 4.8-7.6 sccm Xe, discharge voltage 20-30 V, and discharge current 12-16 A) to simulate NSTAR operating conditions.

ESA Checkout Using an RF Ion Source:

Over a period of operation, the ESA would begin to malfunction. It is believed that this was due to the probe becoming dirty over time and subsequent cleaning of the probe appeared to mitigate this problem. To determine if the probe was malfunctioning, the ESA was directed toward a mono-energetic ion beam produced by an RF ion source. Figure 3 shows ESA traces taken at beam voltages of 50, 70, and 90 V. In general, the most probable energy the ESA measured was consistently about 10 eV lower than the beam voltage, which was expected with xenon gas. Also, the full width half maximum (FWHM) for each distribution was about 10 eV for the RF source. This result was reasonable in that the ESA data was relatively consistent over the energy ranges selected and the current levels were steady. Also, the distributions were more repeatable following a probe cleaning. For the trace at a beam voltage of 50 V (shown in red), a small peak was seen around an energy of 70 eV. It is thought that this peak was possibly due to doubly charged ions that had charge exchanged into singly charged ions once they were outside of the ion source in the beam plasma (~10 V) and then were detected by the ESA.

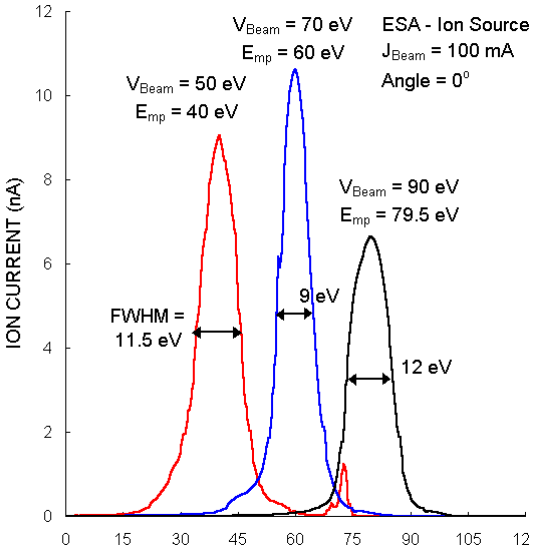

Fig. 3 ESA data of a mono-energetic ion source at different beam voltages.

III. Results

Figure 4a shows an ion energy distribution function measured by the ESA looking at the NSTAR discharge chamber prototype. This measurement is presented as a typical case for most of the traces from the ESA. Viewing the distribution with the linear-linear scale format yields two main signal peaks. The first peak that occurs at an energy of 7 eV is probably due to a large number of charge exchange ions that are produced in the region from the exit of the discharge chamber to the entrance of the ESA. The second peak is believed to be associated with ions produced within the discharge chamber volume. This ion group had most probable energies near the anode potential, in this case a most probable energy of 24.5 eV for this operating condition at a voltage of 24.9 V.

Figure 4b shows the same data set with the y-axis changed to a log scale. Now, two more features of the distribution can be seen in addition to the charge exchange and discharge signal. The first is a shoulder that occurs on the high side of the main discharge signal. At higher energies from 60 to 115 eV in energy, another signal can be distinguished at very low current magnitudes.

One method to characterize the different signals is to assign ion temperatures. For the main discharge signal, this can be done in two ways. The first is to measure the full width half maximum (FWHM). In this case, the FWHM was about 5.3 eV and this gives an ion group temperature of about 3.8 eV (i.e., T_i = (FWHM/2)/ln2). A second way of estimating the ion temperature is to fit an exponential curve to the tail of the ion group where the inverse of the slope yields the ion temperature (typically this method works well when at energies that are several times larger than the ion temperature relative to the energy at the drift velocity). Using this method, the main discharge ions displayed a lower temperature of 1.2 eV, but it is pointed out that the tail of the discharge ion signal

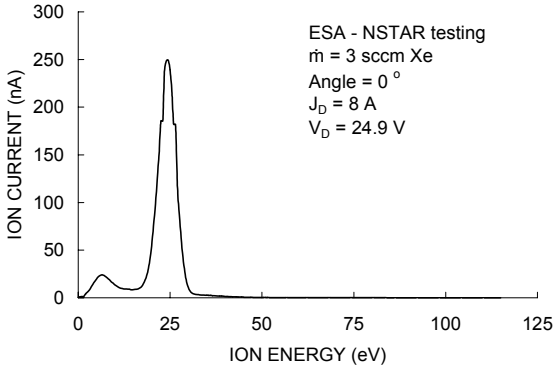

Fig. 4a Typical ESA ion energy distribution function (linear-linear scale).

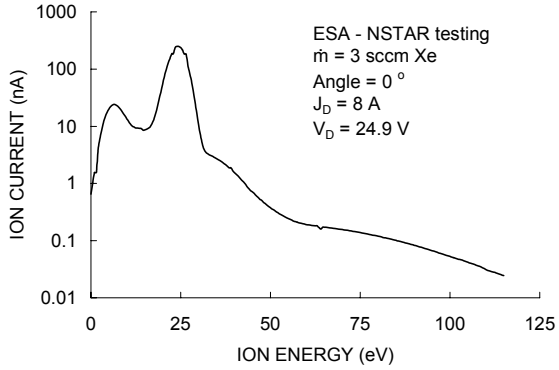

Fig. 4b) Ion energy distribution shown on a log-linear scale.

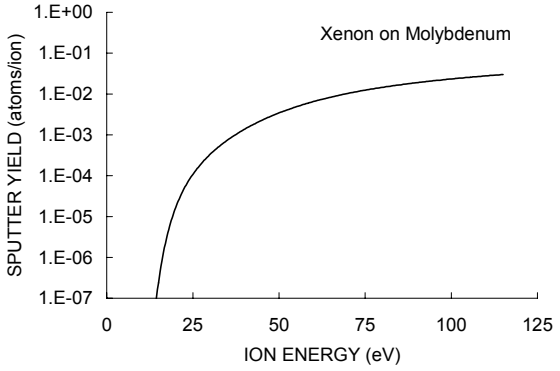

Fig. 4c) Sputter yield data for xenon on molybdenum.

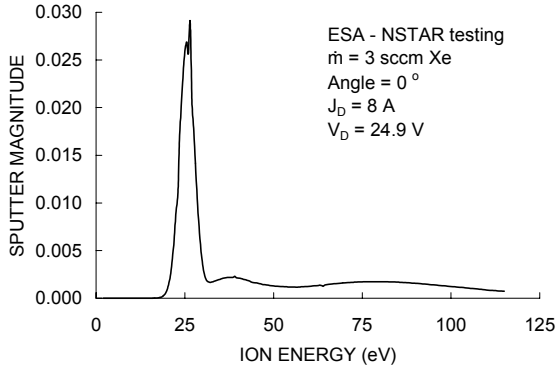

Fig. 4d) Magnitude comparison of sputtering caused by each ion group.

may have been perturbed by the presence of a higher energy group. The separate group of ions in the shoulder of the discharge signal had a much higher temperature of 8 eV. The highest energy ion group that can be identified in Fig. 4b is difficult to characterize with a temperature.

Although the ion energy distribution signal does contain highly energetic ions, the signal strengths associated with these ions are much lower than the main discharge ion signal. To investigate which ion groups may play a significant role in erosion of the discharge chamber components, the ion energy distribution can be multiplied by a corresponding sputter yield measurement. Figure 4c shows the sputtering yield versus energy of xenon ions impinging at normal incidence on a molybdenum surface.[6] Figure 4d shows the result of multiplying the ion energy distribution function by the corresponding sputter yield value. The magnitude represents how much damage each ion group would cause compared to the other groups. In this case and in all of the operating conditions presented in the paper, the discharge ion signal is about an order of magnitude larger than the other groups and would probably cause more damage inside the chamber than the high-energy ion signal. It is noted that these calculations correspond to the location of the ESA. However, the solid angle view factor of the ESA is quite small (0.002 Steradians).

What can be gained from the results presented next is an understanding of how the various groups of ions change in shape (i.e., magnitude and energy) depending on where the ESA is sighted and what operating conditions (flow rate, discharge current, discharge voltage) are chosen.

Angle variation:

The ESA was rotated to different zenith angles to determine how ion energy characteristics change with angle. Figure 5 shows a plot of ion energy distribution functions at four zenith angles of 0º (black), 10º (purple), 20º (blue), and 30º (green). The discharge chamber was operated at a xenon flow rate of 6 sccm and had a discharge current and voltage of 12 A and 24 V, respectively. At this condition, there was a faint high-energy signal at the 20° and 30° angles. For any operating condition chosen, the main discharge ion signal was highest when looking at zero degrees and dropped as the zenith angle was increased, which is probably due to the small acceptance angle of the ESA. In this case, the shoulder of the main discharge signal was present at the zero and 10º angles. Looking at higher ion energies around 60 eV, the current signal was highest when looking at the 20° and 30° angles. At

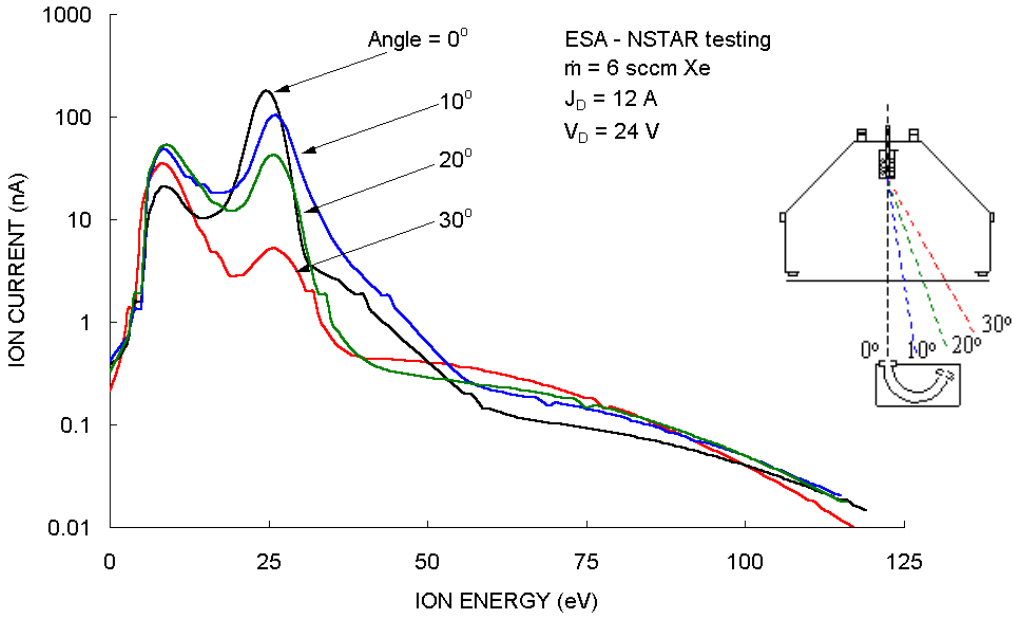

Fig. 5 Effect of zenith angle on the ion energy distribution function.

this condition the discharge ion signal and shoulder were about a factor of 1000 times higher in current magnitude. Due to the large current magnitude, the discharge ions probably have more of an effect on any erosion that might occur inside the discharge chamber.

Position variation:

The ESA was mounted on top of a linear actuator that could move the probe to allow different regions within the discharge chamber to be sampled. This was done to investigate ion energy distributions along a line of sight that did not include the cathode orifice. Figure 6 shows distribution functions taken over a range of –5 cm (left of the cathode) to +5 cm (right of the cathode). The main discharge signal energy and magnitude was very similar for all three traces. The main difference in the traces was in the high-energy ion signal at energies above about 80 eV. For these distributions, the discharge chamber was run at 12 A on the discharge and a 3 sccm flow rate. This condition was selected to produce a more distinct high-energy ion signal. It was thought that the high-energy signal would be best seen at or near the cathode and that is similar to what is shown here. The trace taken at a position of 0 cm had a high-energy signal that was greater in magnitude than the traces taken at –5 and +5 cm.

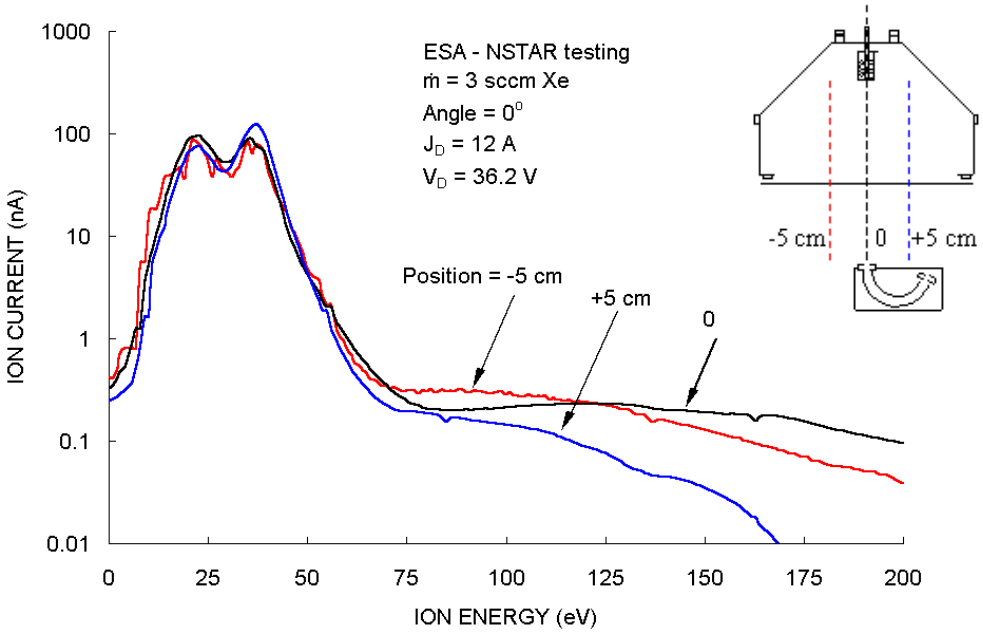

Fig. 6 ESA measurements at positions of –5, 0, and +5 cm.

Discharge current variation:

Varying the discharge current produces a definite change in the ion energy distribution. Figure 7 shows three distributions taken at discharge currents of 8, 10, and 12 A that were plotted on a log-linear plot. For all three distributions, the flow rate was set to 3 sccm Xe and the ESA was pointed at the cathode orifice at a zenith angle of zero degrees. The trace taken at a discharge current of 8 A had a most probable energy of 24.5 eV which corresponded to the discharge voltage of 25 V. As the discharge current was increased, the discharge voltage increased to 27.5 V at a discharge current of 10 A and 36 V at a current of 12 A. The most probable energy of the main discharge signal matched the discharge voltage to within a few eV for all of the traces taken. It is noted that the high-energy ion component increased in both ion energy and magnitude as the discharge current was increased. However, the discharge ion signal was still more significant in terms of erosive power (at the ESA location).

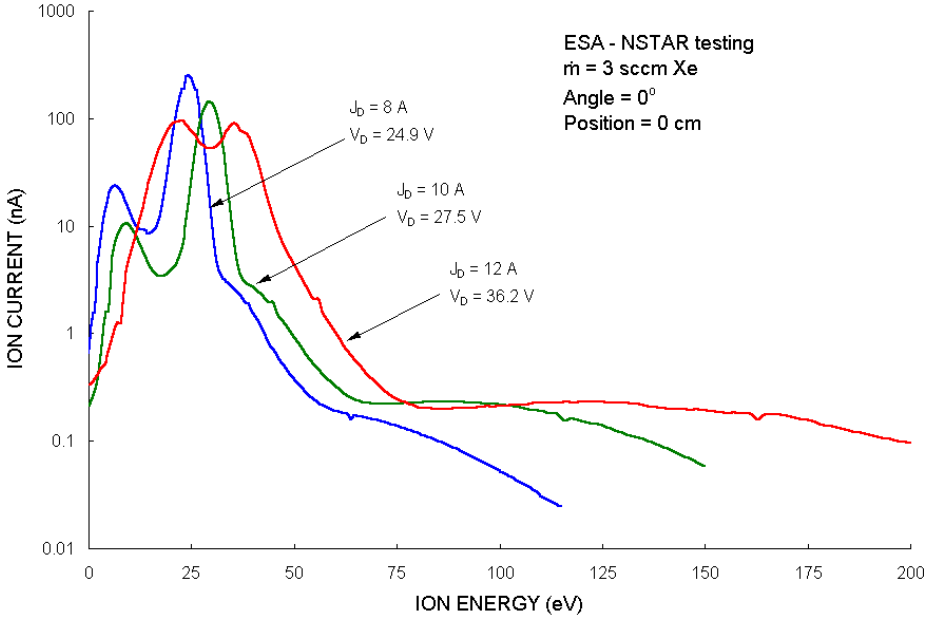

Fig. 7 Effect of discharge current on the ion energy distribution function.

Flow rate variation:

Flow rate also changes the magnitude of the ion energy distribution. Figures 8a and 8b show ion energy distributions at angles of 0 and 30 degrees at three flow rates of 3, 4.5, and 6 sccm Xe. All of the traces were taken at a discharge current of 12 A. The most probable energy of the main discharge ion signal was near the discharge voltage for each flow rate condition, and as the flow rate was increased, the discharge voltage decreased. In a corresponding manner, the shoulder of the main discharge signal also decreased along with the high-energy ion component. The high-energy ion signal was much more pronounced at the lower flow of 3 sccm compared to 6 sccm.

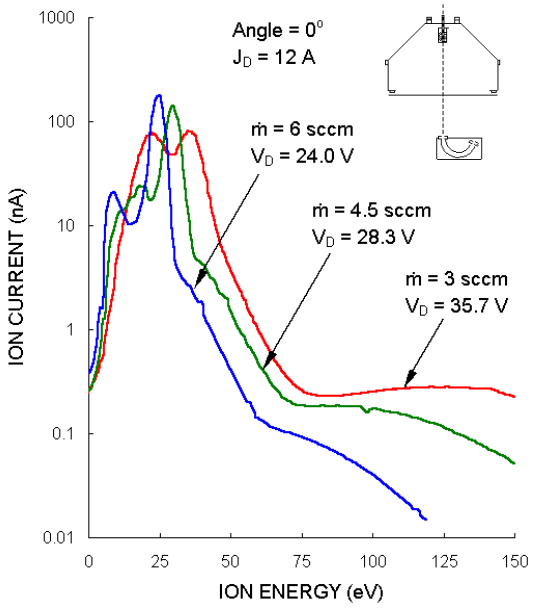

Fig. 8a Flow rate variation at an angle of zero degrees.

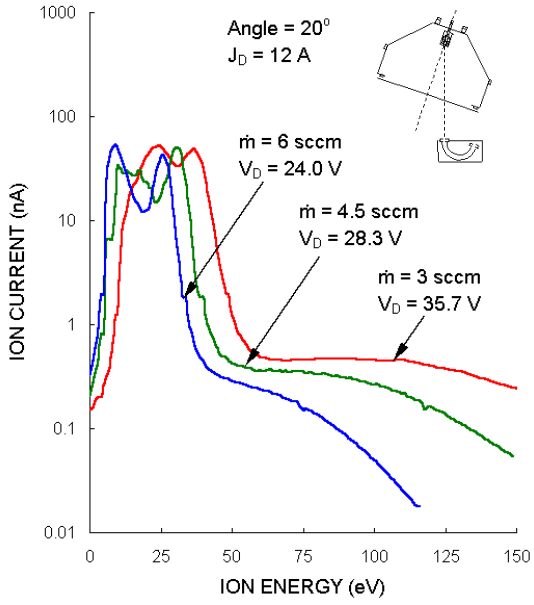

Fig. 8b Flow rate variation at an angle of 20 degrees.

IV. Conclusions

Ion energy distribution measurements were made of ions produced within an NSTAR prototype discharge chamber that stream out through slots cut in the sidewall. The ion energy measurements were performed using an electrostatic analyzer located outside of the discharge chamber. Multiple ion groups were observed in the distribution function. Ion produced within the volume of the discharge chamber at or near anode potential comprised most of the ESA signal (where the most probable ion energy corresponded to the anode voltage), and these ions displayed a relatively high temperature of 3 to 4 eV. In some cases, higher energy ion groups were present with ion energies well above the cathode to anode voltage difference. The effects of changing the operational characteristics of the discharge chamber were studied to investigate ion distribution characteristics. It was found that by increasing the discharge current while keeping the flow rate constant, the most probable energies of the distributions increased along with the discharge voltage. Decreasing the flow rate also produced higher ion energies along with higher discharge voltages. In addition, ion energy distributions were studied as the probe location and angle were varied with respect to the hollow cathode. Varying the zenith angle from 0 degrees (on cathode centerline) to 30 degrees caused the main discharge signal to decrease in current magnitude while the high-energy ion current signal increased. Also, sighting along lines of sight well away from the cathode orifice caused no change in the discharge ion signal but a decrease in the high-energy ion signal. A general conclusion is made that the main discharge ion group (with ion temperatures of 3 to 4 eV) appears to have more of an effect on sputter erosion at the location where the ESA sampled the distribution function. This general result was obtained through the use of recent sputter yield data at low energies that were folded into the ion energy distribution functions made in this study. Future work is recommended where the ESA be moved to locations closer to the hollow cathode to determine volumetric variation in the sputter erosive power of the different ion groups that are detected.

Acknowledgments

Results of this work were generated under the Ion Thruster Lifetime Evaluation Effort under the Prometheus program at the Jet Propulsion Laboratory with direction from Dr. Dan M. Goebel. Financial support from the Jet Propulsion Laboratory is gratefully acknowledged.

References

[1] A. Sengupta, J.R. Brophy, and K.D. Goodfellow, "Status of the Extended Life Test of the Deep Space 1 Flight Spare Ion Engine After 30,352 Hours of Operation," AIAA-2003-4558, 39th Joint Propulsion Conference, Huntsville, AL, 2003.

[2] T. Randolph and J.E. Polk, "An Overview of the Nuclear Electric Xenon Ion System (NEXIS) Activity," AIAA-2004-3450, 40th Joint Propulsion Conference, Fort Lauderdale, FL, July 2004.

[3] J.A. Vaughn, T.A. Schneider, J.E. Polk, D.M. Goebel, W. Ohlinger, D. Hill, "NEXIS Reservoir Cathode 2000 Hour Life Test," AIAA-2004-4203 , 40th Joint Propulsion Conference, Fort Lauderdale, FL, July 2004.

[4] Dan M. Goebel, Kristina K. Jameson, Ron M. Watkins, and Ira Katz, "Hollow Cathode and Keeper-Region Plasma Measurements Using Ultra-Fast Miniature Scanning Probes," AIAA-2004-3430, 40th Joint Propulsion Conference, Fort Lauderdale, July 11-14, 2004.

[5] Casey C Farnell, John D. Williams, and Paul J. Wilbur, "Characteristics of Energetic Ions Emitted From Hollow Cathodes," IEPC-03-072. 28th International Electric Propulsion Conference, Toulouse, France, March 17-21, 2003.

[6] R. P. Doerner, D. G. Whyte, and D. M. Goebel, "Sputtering Yield Measurements During Low Energy Xenon Plasma Bombardment," J. Applied Physics, V. 93, No. 9, pp. 5816-5823, 2003